HEALTH AND MEDICINE

Metabolic fluorine labeling and hotspot imaging of dynamic gut microbiota in mice

Dongxia Chen[1]†, Junnan Guo[1]†, Ao Li[1], Chengjie Sun[1], Huibin Lin[2], Hongyu Lin[1]*, Chaoyong Yang[1,2]*, Wei Wang[2]*, Jinhao Gao[1]*

Real-time localization and microbial activity information of indigenous gut microbiota over an extended period of time remains a challenge with existing visualizing methods. Here, we report a metabolic fluorine labeling (MEFLA)–based strategy for monitoring the dynamic gut microbiota via ^{19}F magnetic resonance imaging (^{19}F MRI). In situ labeling of different microbiota subgroups is achieved by using a panel of peptidoglycan-targeting MEFLA probes containing ^{19}F atoms of different chemical shifts, and subsequent real-time in vivo imaging is accomplished by multiplexed hotspot ^{19}F MRI with high sensitivity and unlimited penetration. Using this method, we realize extended visualization (>24 hours) of native gut microbes located at different intestinal sections and semiquantitative analysis of their metabolic dynamics modulated by various conditions, such as the host death and different β-lactam antibiotics. Our strategy holds great potential for noninvasive and real-time assessing of the metabolic activities and locations of the highly dynamic gut microbiota.

INTRODUCTION

Similar to many other complex biological systems, mammalian gut microbiota is characterized by its high dynamics in distributions, microbial activities, and functions (*1*–*3*). The activities and locations of gut bacteria in different intestinal sections can be influenced by a number of factors, including drug and food intake by the host (*4*, *5*), mobility of the intestines (*6*), and immune factors (*7*), and these changes are also tightly related to the functions carried out by the microbes. Therefore, a noninvasive in situ imaging method, which can gain knowledge of the real-time localization and fluctuant microbial activities of gut microbiota over an extended period of time, is very valuable in furthering our understanding of the physiological/pathological functions of the gut bacteria. Moreover, mammalian gut microbiota is composed of a great diversity of bacterial species (*8*). Therefore, the capability of multiplex and selective imaging of different bacterial groups is also much desired.

In the past decade, several methods for in vivo imaging have been developed for depicting the biodistributions of gut bacteria. One strategy is using antibiotic-tagged probes for noninvasive imaging with high penetration, such as ^{99m}Tc-ubiquicidin for scintigraphy (*9*) and vancomycin-tagged IRDye 800CW for near-infrared (NIR) fluorescence imaging (*10*), which is based on the affinities between antibiotics and bacteria (*11*, *12*). However, the efficacy of this strategy for in vivo imaging of the native microbiota is compromised by the unavoidable disturbance of the antibacterial probes to gut microbes. Another strategy is leveraging the selective uptake of some nutritional compounds by bacteria to deliver imaging probes containing radioactive isotopes (e.g., ^{11}C and ^{18}F). For example, 2-deoxy-2-[^{18}F]fluoro-D-sorbitol (^{18}F-FDS), 2-[^{18}F]fluoro-para-aminobenzoic acid (2-^{18}F-PABA), and [^{11}C]PABA, which could be selectively taken up by bacteria, were used for in situ labeling of the gut microbiota and subsequent in vivo imaging by positron emission tomography–computed tomography (PET-CT) (*13*). Although the viability of this strategy has been demonstrated by its wide usage for in vivo imaging of bacterial infections (*14*–*18*), it suffers from the short imaging window of ^{11}C and ^{18}F (with half-lives of ~20 min and ~2 hours, respectively), technical challenges and high costs of probe syntheses, and incapability in multiplexed imaging. Recently, we reported a strategy exploiting metabolic labeling to incorporate fluorescence imaging probes to gut microbes (*6*). An alkyne-containing D-amino acid (DAA) probe was used to introduce alkynyl groups in situ into the peptidoglycan (PGN) of gut bacteria via the functioning of their L,D-transpeptidase (Ldt) and D,D-transpeptidase (Ddt) (*19*, *20*), which offered a handle for subsequent in vitro incorporation of NIR-II dyes via Cu(I)-catalyzed azide-alkyne cycloaddition (CuAAC) and direct in vivo monitoring in recipient mice after oral transplantation. However, this approach was merely suitable for imaging transplanted bacteria. Therefore, an efficient strategy for in situ labeling and in vivo visualization of indigenous gut microbiota with little disturbance and long imaging window is still being actively pursued.

We envisioned that direct integration of imaging probes into metabolic labeling agents may offer a promising solution. Unfortunately, fluorophores, especially those for NIR-II fluorescence imaging with high penetration, are generally bulky and sometimes chemically sensitive, which prevents efficient in vivo metabolic labeling of bacteria. In contrast, ^{19}F-containing moieties, such as CF_3, OCF_3, and SCF_3, are relatively small and chemically inert, ensuring favorable labeling efficiency and minimal disturbance to gut bacteria. The fluorine labeling of bacteria permits noninvasive in vivo tomographic visualization with ^{19}F magnetic resonance imaging (^{19}F MRI). In the past two decades, ^{19}F MRI is gaining momentum in the fields of molecular imaging (*21*, *22*), cell tracking (*23*, *24*), and drug monitoring (*25*). Unlike traditional ^{1}H MRI that sees ^{1}H nuclei in

[1]Department of Chemical Biology, The MOE Key Laboratory of Spectrochemical Analysis and Instrumentation, Fujian Provincial Key Laboratory of Chemical Biology, and State Key Laboratory of Physical Chemistry of Solid Surfaces, College of Chemistry and Chemical Engineering, Xiamen University, Xiamen 361005, China. [2]Institute of Molecular Medicine, Shanghai Key Laboratory for Nucleic Acid Chemistry and Nanomedicine, Renji Hospital, Shanghai Jiao Tong University School of Medicine, Shanghai 200127, China.
†These authors contributed equally to this work.
*Corresponding author. Email: hylin007@xmu.edu.cn (HongyuLin); cyyang@xmu.edu.cn (C.Y.); wwang@shsmu.edu.cn (W.W.); jhgao@xmu.edu.cn (J.Ga.)

organisms (mostly in the form of H_2O), ^{19}F MRI visualizes imaging probes containing ^{19}F atoms, which are of 100% natural abundance, outstanding magnetic resonance (MR) sensitivity (second to ^{1}H among stable isotopes) (*26*), and negligible biological background ($<10^{-6}$ M). Therefore, ^{19}F MRI is emerging as a promising means for visualizing biomolecules and cells that are relatively rare in deep tissues of living subjects, which is challenging for ^{1}H MRI due to high biological background (*27*, *28*). Moreover, the stability of ^{19}F allows for facile and economic probe synthesis and storage (*29*) and grants a much longer imaging window than many radioisotopes, allowing extended monitoring of the dynamics of gut microbiota. Furthermore, the broad range of ^{19}F chemical shift [>350 parts per million (ppm)] and the quantitative nature of MR permits efficient multiplexed imaging with quantification (*30*–*35*), facilitating the studies involving microbes of diverse species. These merits make labeling-enabled ^{19}F MRI an appealing technique for the research community of gut microbiota. In light of these considerations, here, we developed a ^{19}F-labeling strategy termed metabolic fluorine labeling (MEFLA), which exploited metabolic labeling agents containing ^{19}F-containg moieties. This strategy allows for efficient in situ ^{19}F labeling of PGN in mouse gut microbes, enabling multiplexed, extended, and selective in vivo imaging/monitoring of indigenous gut microbiota and semiquantitative analysis of their activities by ^{19}F MRI.

RESULTS

Preparation and characterization of ^{19}F-modified DAA probes

Three ^{19}F-modified DAA (^{19}F-DAA) probes containing six, two, and three fluorine atoms of different chemical shifts were designed and synthesized (see Fig. 1A for chemical structures and fig. S1 for detailed synthesis). Their chemical shifts, as determined by ^{19}F nuclear MR (^{19}F NMR) spectroscopy, were −62.64, −109.60, and −42.78 ppm, respectively (Fig. 1B). Their ^{19}F NMR signals could be simultaneously detected without any mutual interference (Fig. 1B), demonstrating the potential for multichannel ^{19}F MRI. We then measured the longitudinal (T_1) and transverse (T_2) relaxation times of the probes using inversion recovery and Carr-Purell-Meiboom-Gill sequences. All three probes showed relatively long T_2 and short T_1 (table S1), which was favorable for strong ^{19}F MRI signals.

To ensure prolonged in vivo labeling and imaging, we evaluated the stabilities of the three probes in acidic (pH = 1) and basic (pH = 9) aqueous solutions, which mimicked the local environments of stomach and small intestines, respectively. ^{19}F NMR spectra showed no notable changes in ^{19}F signal intensity and chemical shift (fig. S2), demonstrating the high stabilities of the probes in these environments. Furthermore, to assess the potential microbial toxicities of the ^{19}F-DAAs, we tested their effects on the viabilities of different bacteria, including *Bacillus subtilis*, *Staphylococcus aureus*, and *Escherichia coli*. The bacteria were incubated with different ^{19}F-DAAs (final fluorine concentration of 60 or 120 mM) at 37°C for 3 hours, and their survivals were then evaluated by colony-forming unit (CFU) plate counting. None of the probes showed noticeable toxicity (fig. S3), indicating their good compatibilities with bacteria.

Labeling bacterial species in vitro

We next explored the in vitro labeling of bacteria with ^{19}F-DAA. Both Gram-positive (*B. subtilis* and *S. aureus*) and Gram-negative bacteria (*E. coli*) were tested for ^{19}F-DAA labeling using fluorinated L-amino acid (^{19}F-LAA) probes as controls. Neither ^{19}F-DAA nor ^{19}F-LAA probes showed any apparent cytotoxicity (fig. S3). These ^{19}F-LAAs are of the same constitutions with their ^{19}F-DAA counterparts but of different configurations at the chiral centers (see fig. S4 for chemical structures), which thus could not label bacteria via the mechanism of DAA-based labeling (*19*). The three bacterial species were incubated with different probes (final fluorine concentration of 1.2 mM) for 3 hours and subjected to ^{19}F NMR (Fig. 1C and fig. S5). As expected, Gram-positive bacteria showed more efficient labeling than Gram-negative bacteria. This is consistent with previous fluorescent DAA labeling results (*36*, *37*) and can be explained by the fact that the PGN layers of Gram-positive bacteria are much thicker than those of Gram-negative bacteria. Further quantitative analysis of the results revealed that the number of labeled fluorine was ~10^8 atoms per bacterium (see table S2 for calculation). Next, we made a mixture of the three ^{19}F-DAA probes and used this mixture to label different bacteria. No interferences among ^{19}F NMR peaks were observed (fig. S6), implicating the feasibility of visualizing different gut microbes with multichannel ^{19}F MRI. We also investigated the dose-dependent and bacterial quantity-dependent effects of ^{19}F probe labeling. The results indicated positive correlations between ^{19}F signals and incubating concentrations of the ^{19}F probes and between ^{19}F signals and bacterial quantities (figs. S7 and S8). We further explored the influence of cell division on ^{19}F labeling. As shown in fig. S9, although the average ^{19}F signals for a single bacterium kept decreasing as the bacteria continued to divide, the total amount of ^{19}F in all bacteria did not change markedly, indicating that the loss of ^{19}F from the labeled bacteria was negligible.

Multichannel tracking of different bacterial species transplanted to the gut

With the labeling efficiency and multiplexing capability of ^{19}F-DAA probes confirmed, we set out to perform in vivo tracking of bacteria via ^{19}F MRI. Three bacterial species labeled by ^{19}F-DAA probes in vitro (^{19}F-DAA-1 to ^{19}F-DAA-3 for *E. coli*, *B. subtilis*, and *Enterococcus faecium*, respectively; with an incubating fluorine concentration of 6.0 mM) were transplanted to recipient mice (BALB/c) by gavage, which were then subjected to ^{19}F MRI (Fig. 1D). Real-time multichannel ^{19}F MRI, together with ^{1}H MRI, showed that the localizations of the three bacteria could be tracked simultaneously (Fig. 1E). Most microbes were still in the stomach 2 hours after gavage and translocated to the intestines at 6 hours, where the two Gram-positive bacteria were of similar translocating patterns. The transplanted bacteria after gavage, especially the two Gram-positive species, could be observed, the signals of which could last for at least 12 hours. In contrast, when the mice were transplanted with ^{19}F-labeled bacteria that had been killed by ethanol, ^{19}F signals rapidly dissipated in the intestines after passing the stomach and accumulated in the bladder (fig. S10), indicating that dead ^{19}F-labeled bacteria quickly lose their labeling in vivo, probably due to the degradation of their cell walls. These results demonstrate the great potential of our strategy for noninvasive real-time in vivo imaging and monitoring of multiple types of

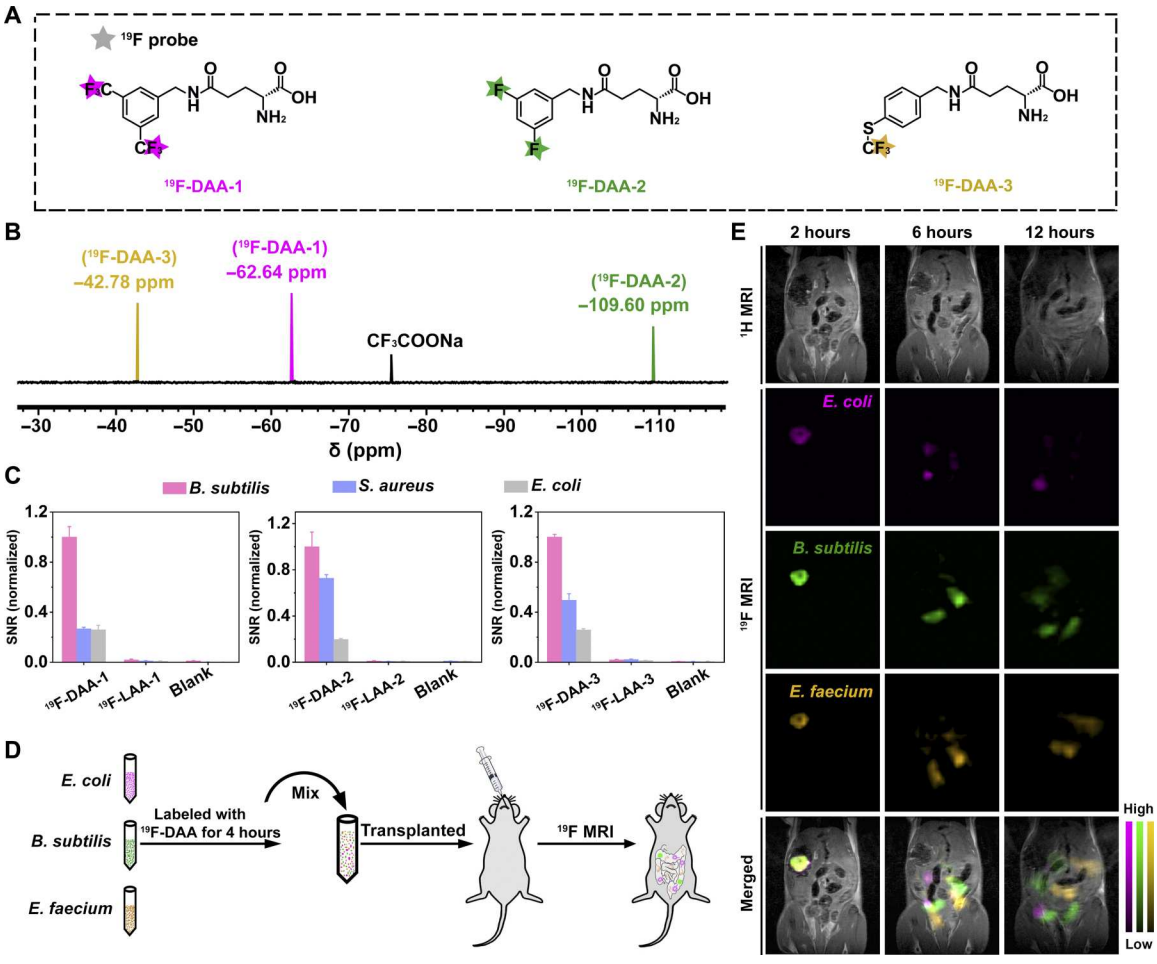

Fig. 1. Structures and chemical shifts of ^{19}F-DAA probes and multiplexed ^{19}F MRI of different bacteria labeled in vitro and subsequently transplanted via gavage. (**A**) Chemical structures of ^{19}F-DAA probes. (**B**) A ^{19}F NMR spectrum of a mixture containing three ^{19}F-DAA probes. Fluorine concentrations for ^{19}F-DAA-1 to ^{19}F-DAA-3 in the mixture were 1.2, 1.0, and 1.0 mM, respectively. ppm, parts per million. (**C**) Quantitative ^{19}F NMR signal-to-noise ratio (SNR) analysis of indicated bacteria labeled by ^{19}F-DAA probes. ^{19}F-LAA probes and phosphate-buffered saline were used as controls. Different bacteria were labeled with each probe individually at a fluorine concentration of 1.2 mM. The maximum SNR for each set of samples was normalized as 1.0, and the other SNRs were scaled accordingly (n = 5 per group, graph bars = mean, and error bars = SD). (**D**) Schematic illustration of in vivo multichannel bacterial tracking. Three bacterial species separately labeled by the three ^{19}F-DAA probes for 4 hours (^{19}F-DAA-1 to ^{19}F-DAA-3 for *E. coli*, *B. subtilis*, and *E. faecium*, respectively, at a fluorine concentration of 6.0 mM) were mixed and transplanted to recipient mice by gavage, which were then subjected to ^{19}F MRI. (**E**) Multiplexed hotspot ^{19}F MRI for tracking the transplanted bacteria in vivo within 12 hours after gavage.

transplanted bacteria used as living probiotics or in pathogen research (*38*–*40*).

In vivo labeling of gut microbiota

After completing the in vivo tracking of bacterial species ^{19}F-tagged in vitro, we attempted to label mouse gut microbiota in situ with ^{19}F-DAA. First, each of ^{19}F-DAAs was given to mice by gavage, whose cecal microbiotas were collected after 6 hours (bacterial compositions analyzed by 16*S* ribosomal DNA sequencing; fig. S11) and then analyzed by ^{1}H/^{19}F MRI (Fig. 2A). The cecal microbiotas labeled by ^{19}F-DAAs all displayed strong ^{19}F MRI signals, while the ^{19}F-LAA controls showed no noticeable labeling (Fig. 2B), indicating that ^{19}F-DAA probes could effectively label mouse gut microbiota in vivo. Next, we used a mixture of the three ^{19}F-DAA probes for gavage (indicated by a white arrow; Fig. 2B) and found that the ^{19}F MRI signals of the three probes could all be observed, showing that the three probes could simultaneously label gut bacteria in vivo, and be visually distinguished. The influences of the ^{19}F probes on the metabolic activities of gut microbiotas were also investigated (see fig. S12 and the Supplementary Materials for details). No significant impacts were found.

We then performed fecal microbiota transplantation (FMT), an operation that was frequently conducted in microbiota research. The ^{19}F-labeled microbiota was used as donor bacteria, and their localization in the gut was tracked with ^{19}F MRI. Previously, we reported a NIR-II fluorescence-based labeling and tracking strategy for FMT (6). This approach required the donor microbiota to be further tagged with NIR-II fluorophores in vitro before transplantation, which prolonged their exposure to aerobic environments, resulting in a potential compromise of their viability because most commensal gut bacteria were obligately anaerobic. In contrast, the gut microbiota labeled with ^{19}F-DAA-1 could be directly used in

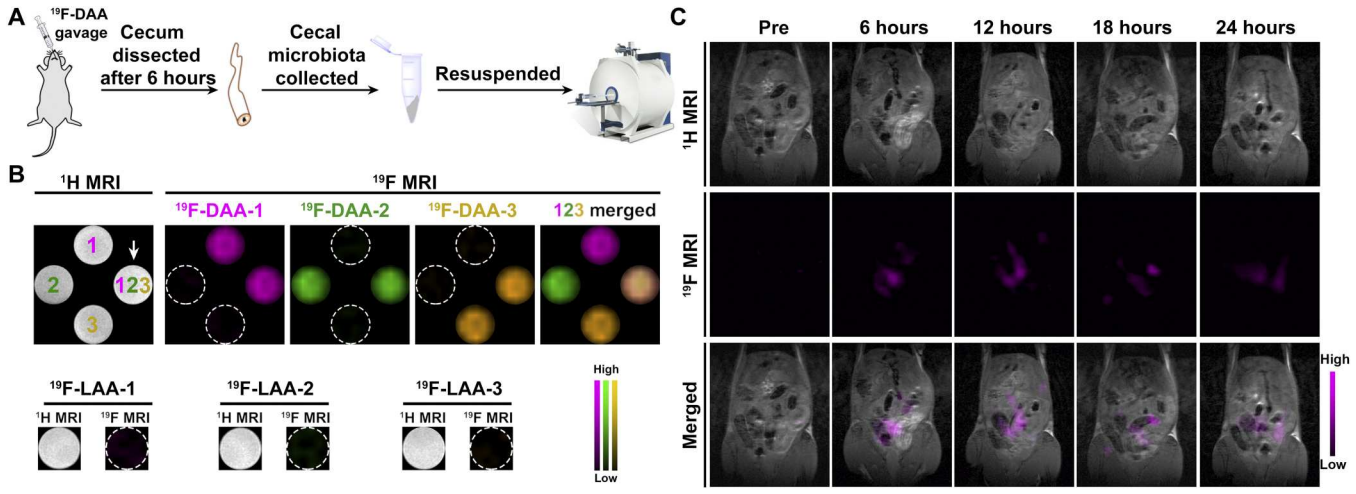

Fig. 2. In vivo metabolic labeling of gut microbiota with ^{19}F-DAA probes and tracking the localization of ^{19}F-labeled bacteria after transplantation by ^{19}F MRI. (**A**) Schematic illustration of in vivo metabolic labeling of gut microbiota with ^{19}F-DAA probes. (**B**) ^{1}H MRI and multichannel ^{19}F MRI of gut microbiotas labeled with either one of the ^{19}F-DAA probes or a mixture of three probes in vivo. Microbiotas treated with corresponding ^{19}F-LAA probes were used as controls. (**C**) ^{19}F MRI of a mouse after receiving intragastric transplantation of the gut microbiota labeled with ^{19}F-DAA-1.

FMT, and the transplanted bacteria could be monitored in vivo for more than 24 hours by ^{19}F MRI (Fig. 2C), offering a more efficient method for extended in vivo tracking of donor microbiotas in FMT.

Multiplexed ^{19}F MRI of indigenous gut microbiota

After demonstrating the feasibility of in vivo tracking of transplanted microbiota, we then explored whether we could label and visualize indigenous gut microbiota in situ. One of the ^{19}F-DAA probes (^{19}F-DAA-3) was used for mouse gavage, and ^{19}F-LAA-3 was used as a control. In the first 1 hour, strong ^{19}F MRI signals could be observed in the stomach for both ^{19}F-LAA– and ^{19}F-DAA–treated mice (Fig. 3, A and B), which could be ascribed to the high-concentration probes in the stomach after gavage. In the ^{19}F-LAA–treated mouse, ^{19}F signals markedly diminished in the digestive tracts and started to appear in the bladder at 4 hours after gavage (Fig. 3B and fig. S13). This phenomenon could be attributed to the nonspecific absorption of ^{19}F-LAA-3 by the host, leading to the attenuation of ^{19}F MRI signals in the gut. The ^{19}F signals in the bladder probably resulted from the urinary excretion of the ^{19}F-LAA probe, which had been observed in a previous report (*41*). In contrast, strong ^{19}F MRI signals were retained in the intestines of the ^{19}F-DAA–treated mouse even at 12 hours (Fig. 3A). Given that free DAA probes could also be absorbed by the host and excreted via urine (*41*), which was also observed for ^{19}F-DAA-3 at 4 hours (Fig. 3A), the signal retention in the intestines was attributed to the ^{19}F labeling of the gut microbiota.

To verify this speculation, swe collected the mouse cecal microbiotas at 24 hours after ^{19}F-DAA-1 gavage and compared the ^{19}F MRI signals of the bacterial suspensions with or without washing to remove free ^{19}F-DAA-1. No substantial differences in signal intensity were observed between two groups (fig. S14), indicating that the ^{19}F MRI signals detected were from ^{19}F-DAA–labeled bacteria and that most of excess probes were cleared by the host, which ensured minimal background interference. To further confirm this result, we performed another control experiment using a modified ^{19}F-DAA-1 probe (^{19}F-DAA-1-Ac) for gavage, whose primary amino group was acetylated, leading to its inability in labeling bacteria (*20*). A pattern of ^{19}F MRI signals similar to that of the ^{19}F-LAA–treated mice was observed (Fig. 3C), suggesting its failure in labeling the bacteria. Moreover, when in vivo ^{19}F-DAA labeling was performed in germ-free (GF) mice, no ^{19}F MRI signals were observed at 6 hours after gavage (Fig. 3D), indicating the clearance of the probes by the host without any interactions with the gut microbiota. Together, the ^{19}F MRI signals observed in the gut at 4 hours after gavage were from the gut microbiota labeled by ^{19}F-DAA, demonstrating the successful in situ labeling and imaging of indigenous gut microbes.

Next, by taking advantage of the multiplexing capability of ^{19}F MRI, we carried out sequential ^{19}F-DAA labeling of the gut microbiota. The three ^{19}F-DAA probes were successively used in gavage at 6-hour intervals, aiming to label and visualize bacteria located at different sections of the intestines. As shown in Fig. 3E, multichannel ^{19}F MRI signals could be observed. The detecting time window for each probe was up to 24 hours, allowing for more extended imaging analysis than ^{18}F labeling–based bacterial visualization (*20*). In the merged image at 24 hours, the relative locations of bacteria labeled by the three probes could be readily visualized, illustrating the potential of our approach for multiplexed in situ labeling and imaging.

Tetrapeptide-based selective ^{19}F labeling of gut microbiota

As a universal PGN-targeting probe, DAA probes can label most types of bacteria (*37*). We further investigated the selective ^{19}F labeling of gut microbiota that could target a specific subgroup of bacteria and accomplish selective ^{19}F MRI. Inspired by a fluorescent tetrapeptide probe (tetraAA) previously developed by Pires *et al.* (*42*) and recently adopted by our group for selective labeling of a subgroup of Gram-positive bacteria in vivo (*43*), we designed and synthesized a ^{19}F-tagged tetrapeptide probe (^{19}F-tetraAA; see Fig. 4A for its chemical structure). By mimicking the substrate for Ldts (an enzyme constructing 3-3 cross-links in PGN) that existed in some of the Gram-positive bacteria, this tetrapeptide probe could

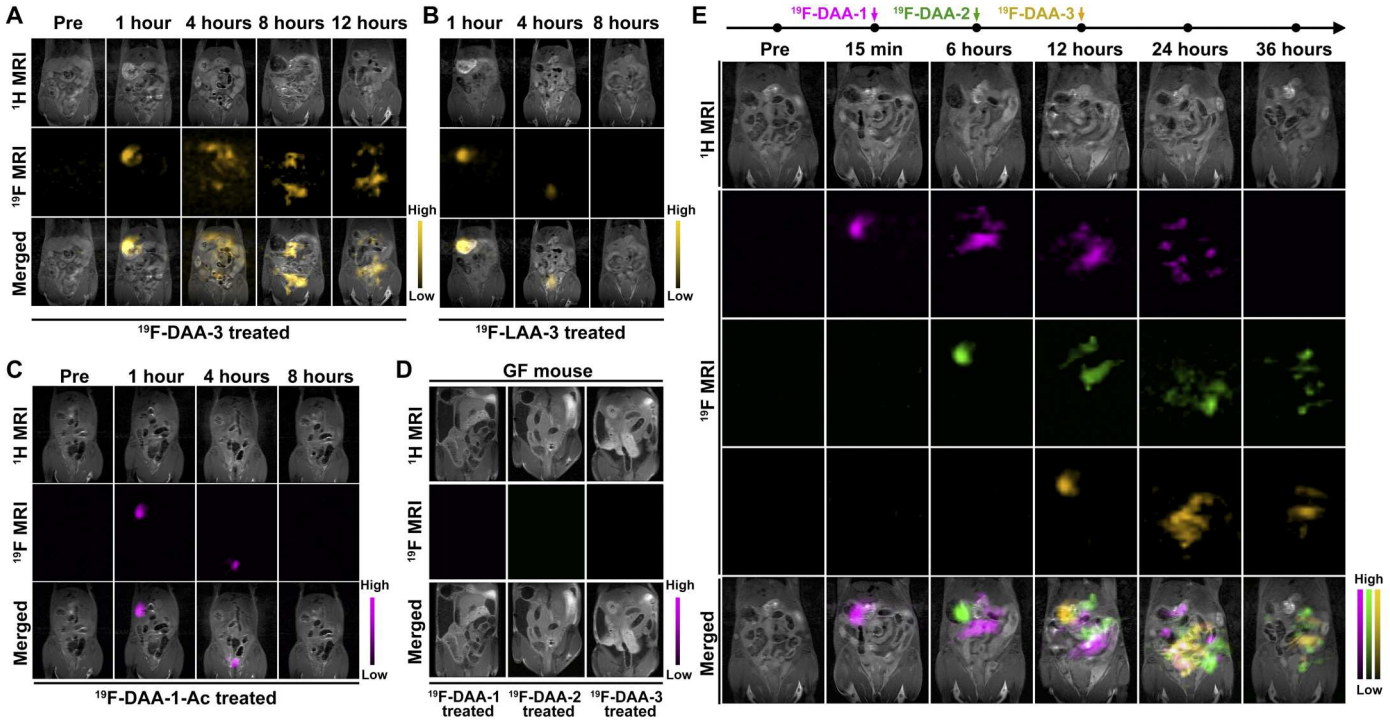

Fig. 3. In vivo visualization of indigenous gut microbiota via ^{19}F MRI. Real-time ^{19}F MRI of gut microbiota treated with ^{19}F-DAA-3 (**A**), ^{19}F-LAA-3 (**B**), or ^{19}F-DAA-Ac (**C**). (**D**) ^{19}F MRI of GF mice at 6 hours after gavage with ^{19}F-DAA-1 to ^{19}F-DAA-3. (**E**) Multichannel and prolonged visualization of the native gut microbiota of a mouse sequentially labeled with three ^{19}F-DAA probes at 6-hour intervals by hotspot ^{19}F MRI.

be specifically recognized by the enzyme and covalently tagged to PGN via 3-3 cross-links (see fig. S15 for labeling mechanism). A control probe (*ctrl*-^{19}F-tetraAA) was used for comparison, the configuration of the fourth amino acid of which was different from that of ^{19}F-tetraAA (Fig. 4A, indicated in blue), resulting in the failure of recognition by Ldts. No notable cytotoxicity was found for either ^{19}F-tetraAA or *ctrl*-^{19}F-tetraAA (fig. S3).

We first explored the in vitro labeling efficiency of *E. faecium*, *B. subtilis*, and *E. coli* with ^{19}F-tetraAA. ^{19}F NMR showed that ^{19}F-tetraAA could effectively label *E. faecium* but not *B. subtilis* or *E. coli*, both of which had meso-diaminopimelic acid but not L-Lys on the stem peptides' third position, while the *ctrl*-^{19}F-tetraAA failed to generate any noticeable labeling to any of the three bacteria (Fig. 4B and fig. S16), demonstrating the labeling specificity of ^{19}F-tetraAA. Next, we performed in vivo labeling of mouse gut microbiota with orally administered ^{19}F-tetraAA. The cecal microbiotas collected from the mice treated with ^{19}F-tetraAA at 6 hours after gavage exhibited strong ^{19}F MRI signals, while those collected from the mice treated with *ctrl*-^{19}F-tetraAA did not, implicating the effective in vivo labeling of cecal microbiotas with ^{19}F-tetraAA (fig. S17A).

After confirming the in vitro and in vivo labeling capability of ^{19}F-tetraAA, we explored the selective in situ labeling and imaging of Ldt-expressing Gram-positive bacteria with ^{19}F-tetraAA. Mice were administered with ^{19}F-tetraAA or *ctrl*-^{19}F-tetraAA ([F] = 42 mM, 200 μl) through gavage. Subsequent ^{19}F MRI uncovered strong signals in the stomach of ^{19}F-tetraAA treated mice at 2 hours after gavage and at different locations along the intestinal tracts during 4 to 12 hours, suggesting the accomplishment of in situ labeling and imaging with ^{19}F-tetraAA. By contrast, in the mice treated with *ctrl*-^{19}F-tetraAA, ^{19}F MRI signals was observed in the stomach at 1 hour after gavage and soon translocated to the bladder and disappeared (Fig. 4C), which were very similar to our previous results of in vivo labeling with ^{19}F-LAA and ^{19}F-DAA-1-Ac (Fig. 3, B and C), indicating the failure in labeling gut bacteria. Moreover, when GF mice were administered with ^{19}F-tetraAA, no obvious signals were observed at 6 hours after gavage (fig. S17B). Collectively, these results demonstrate the success of our approach for specific in vivo labeling and imaging of a subgroup (Ldt-expressing Gram-positive bacteria) of the gut microbiota with ^{19}F-tetraAA.

Multiplexed ^{19}F MRI of different groups of indigenous gut microbiota in vivo

With the capability of ^{19}F-tetraAA for in vivo labeling and imaging confirmed, we coadministered two probes, ^{19}F-tetraAA and ^{19}F-DAA-3, to mice in attempt to image different groups of gut microbes simultaneously (Fig. 5A). After gavage, the ^{19}F MRI signals of the two probes could be readily visualized and differentiated. The distinct distributions of the signals suggest that Ldt-expressing Gram-positive bacteria might have a special distribution pattern in the gut (Fig. 5B). As expected, the signals of ^{19}F-DAA-3 were more intense than those of ^{19}F-tetraAA despite its lower fluorine concentration in gavage, which could be attributed to its broader labeling coverage of bacteria (Fig. 5C) (*43*). These results corroborate the feasibility of our approach, which involves selective in situ labeling with targeting probes and subsequent multichannel ^{19}F MRI, for visualizing distributions of different subgroups of gut

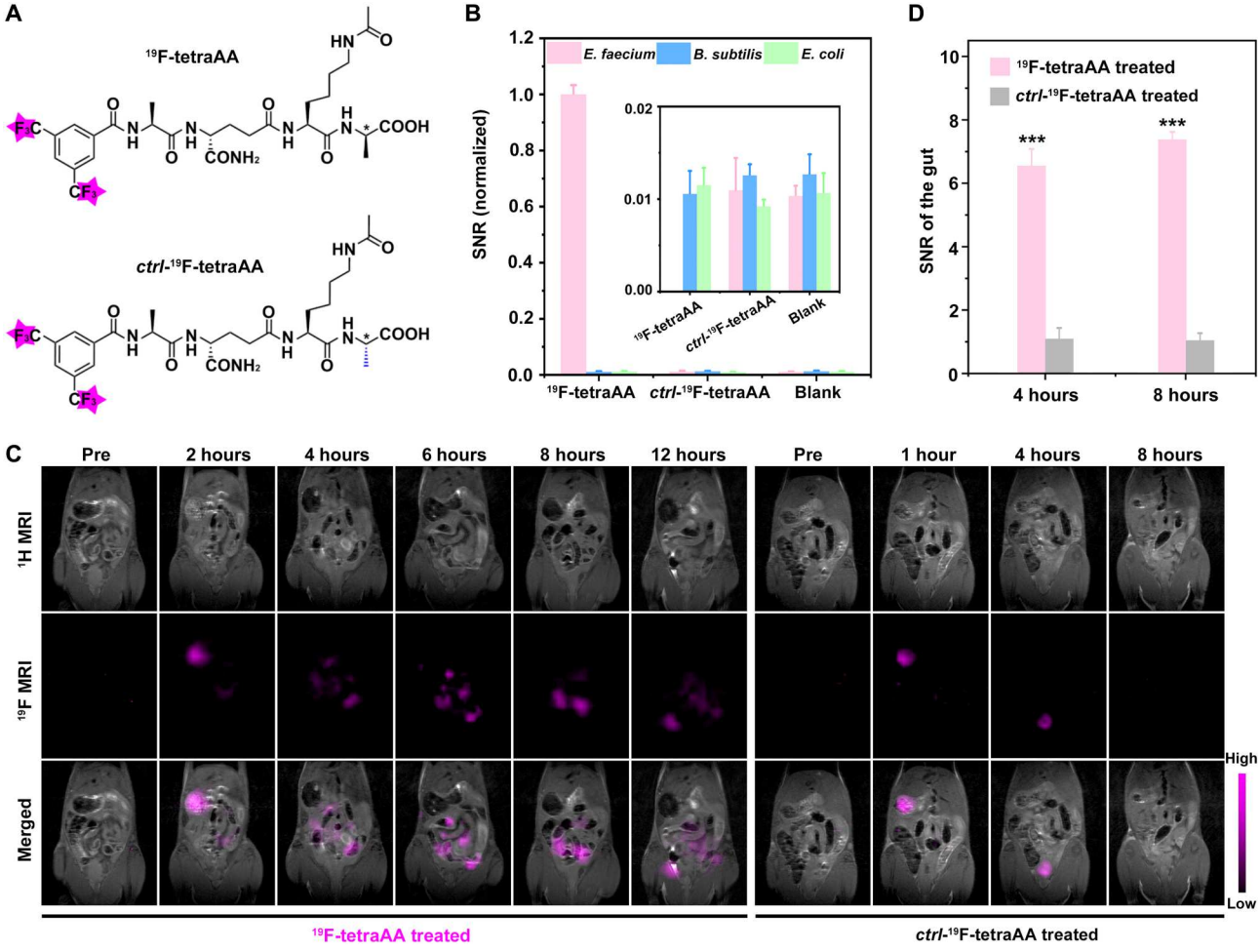

Fig. 4. Tetrapeptide-based metabolic labeling of different bacteria in vitro and ^{19}F MRI of the labeled microbiota in vivo. (**A**) Chemical structures of ^{19}F-tetraAA and *ctrl*-^{19}F-tetraAA. The different chiral center is indicated in blue. (**B**) Relative labeling efficiency of *E. faecium*, *B. subtilis*, and *E. coli* labeled with ^{19}F-tetraAA (n = 5 per group, graph bars = mean, and error bars = SD). (**C**) In vivo real-time and continuous monitoring of the gut microbiota treated with ^{19}F-tetraAA or *ctrl*-^{19}F-tetraAA by ^{19}F MRI. (**D**) Semiquantitative SNR analysis corresponding to (C). n = 3 per group. All data are reported as means ± SD. Statistical significance was calculated using Student's t test for unpaired data, and a P value of less than 0.05 was accepted as an indicator of a statistically significant difference compared to controls (*P < 0.05, ***P < 0.001).

microbiota. Notably, no apparent side effects or histologic changes were observed in the mice treated with our probes, indicating their good biocompatibility (fig. S18).

Continuous monitoring of the gut microbiota dynamics by ^{19}F MRI

Previously, we demonstrated that the signal intensities of fluorescent DAA-labeled gut bacteria could reflect their in vivo metabolic status (*44*). Here, we further explored the use of ^{19}F MRI for directly monitoring the in vivo metabolic dynamics of bacteria. In forensic microbiology, an emerging field of forensic science, the changes in composition, metabolism, and spatial distributions of host microbes are extensively investigated for clues and evidences (*45*, *46*). Our understanding of how gut microbiota is influenced right after the host death, however, is still limited because of the lack of suitable tools for noninvasive in vivo assessment of the microbial system. We envisioned that this ^{19}F MRI–based strategy might offer a potential solution for this problem. Toward this end, we administered three ^{19}F-DAA probes successively at 6-hour intervals to mice via gavage and euthanized the mice at 6 hours after the third gavage. Subsequent ^{19}F MRI unveiled no obvious changes in the intestinal locations and intensities of ^{19}F MRI signals for any of the three channels within 6 hours after the death of the host (Fig. 6A and fig. S19A). These results indicate that the gut microbiota probably maintains a similar level of cellular metabolism in the first 6 hours after the death of the host and preserves the original localization owing to the lack of gastrointestinal movements, which may offer the insights for understanding the changes of gut microbiota in forensic science.

Another frequently explored topic in gut microbiota research is how different antibiotics affect the activities of various bacterial groups in vivo, a process that may lead to microbiota dysbiosis and the spread of antibiotic resistance (*47*, *48*). Compositional changes of fecal microbiotas after antibiotic use determined by DNA sequencing are often used to investigate these effects. Continuous in vivo monitoring and imaging of how antibiotics influence gut microbiota in a real-time manner, however, has seldom been achieved because of the lack of effective techniques *(49)*.

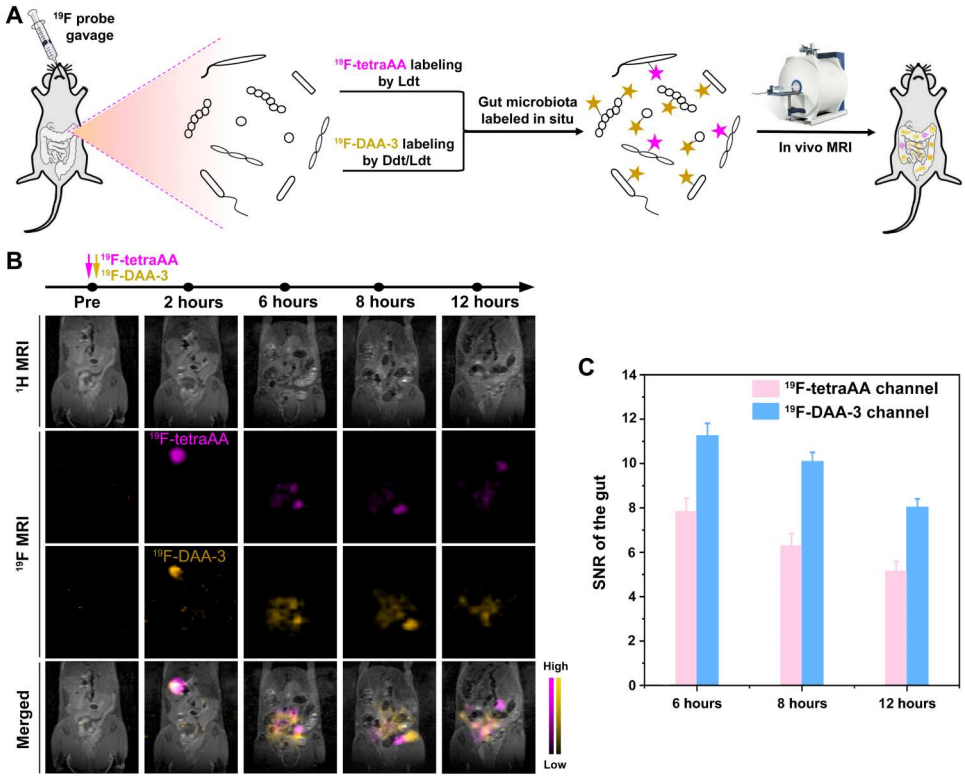

Fig. 5. Multiplexed ^{19}F MRI of different groups of indigenous gut microbiota in vivo. (**A**) Schematic illustration of the workflow for multiplexed ^{19}F MRI. (**B**) Continuous multichannel ^{19}F MRI of the mouse gut microbiota after simultaneous labeling with ^{19}F-tetraAA and ^{19}F-DAA-3. (**C**) Semiquantitative SNR analysis corresponding to (B). *n* = 3 per group, graph bars = mean, and error bars = SD.

The transpeptidase for incorporating ^{19}F-tetraAA, Ldt, unlike the more common Ddts (also named as penicillin-binding proteins), is known to be resistant to most β-lactam antibiotics except carbapenems (functioning mechanism shown in Fig. 6B) (*43*, *50*). In this consideration, we explored the feasibility of our strategy for monitoring the potentially distinct responses of gut microbes to different β-lactams. We coadministered ^{19}F-tetraAA with different types of β-lactams, oxacillin (OX; Ldts ineffective) or imipenem (IPM; Ldts effective), to mice via gavage. Subsequent ^{19}F MRI (Fig. 6C) and semiquantitative signal-to-noise ratio (SNR) analysis (fig. S19B) uncovered no obvious differences in ^{19}F MRI signal for the mice receiving no antibiotic (Fig. 6C, left) and the mice treated with OX (Fig. 6C, middle). However, the ^{19}F MRI signals of the IPM-treated mice decreased considerably, resulting in barely noticeable signals at 6 hours after gavage and undetectable signals after 8 hours (Fig. 6C, right), which is consistent with the fact that IPM (a carbapenem), but not OX (a penicillin), could inhibit Ldts well and prevent effective labeling with ^{19}F-tetra AA. These observations are consistent with the functioning mechanisms of these two β-lactams toward Ldts (Fig. 6B). To the best of our knowledge, this experiment is the first demonstration of a real-time and continuous observation of how gut microbes is influenced by foreign chemicals such as orally administered β-lactam class antibiotics. These results illustrate the potential of our method for direct investigation of the in vivo metabolic activities of gut microbes, which is formidably challenging to address with other existing methods.

DISCUSSION

Because of the difficulties in culturing and genetic engineering of gut bacteria and the lack of proper tools to monitor their in situ activities, obtaining information of the spatial distributions and metabolic activities of gut microbiota in vivo has been notoriously difficult. Here, we established a strategy for in situ labeling and in vivo imaging of gut microbiota. In our approach, a series of PGN-targeting MEFLA probes was used to label gut bacteria, which were then subjected to multiplexed and extended monitoring via ^{19}F MRI. This strategy enables efficient selective in situ labeling of gut microorganisms with stable ^{19}F atoms, which grants a >24-hour observation window for indigenous gut microbiota, permitting continuous monitoring of the microbiota dynamics influenced by many factors, such as physiological conditions (body temperature, aging, exercise, emotional stress, etc.) and ingested substances (nutrients, drugs, poisons, etc.). For example, the imaging window for gut microbiota labeled in vivo by ^{19}F-DAA probes was about 30 hours as indicated in Fig. 3. The semiquantitative capacity of ^{19}F MRI allows for accurate assessment of the activities of labeled microbes. In addition, the multiplexing capability of ^{19}F MRI facilitates simultaneous monitoring of differently labeled bacterial groups in mice. Therefore, our approach opens an avenue for furthering our understanding of the interactions between the host and the gut microbiota and among different bacterial groups.

Our current approach inevitably has some limitations. Our probes allow for broad-spectrum labeling, and thus their selectivity is relatively low. This drawback could be overcome by the

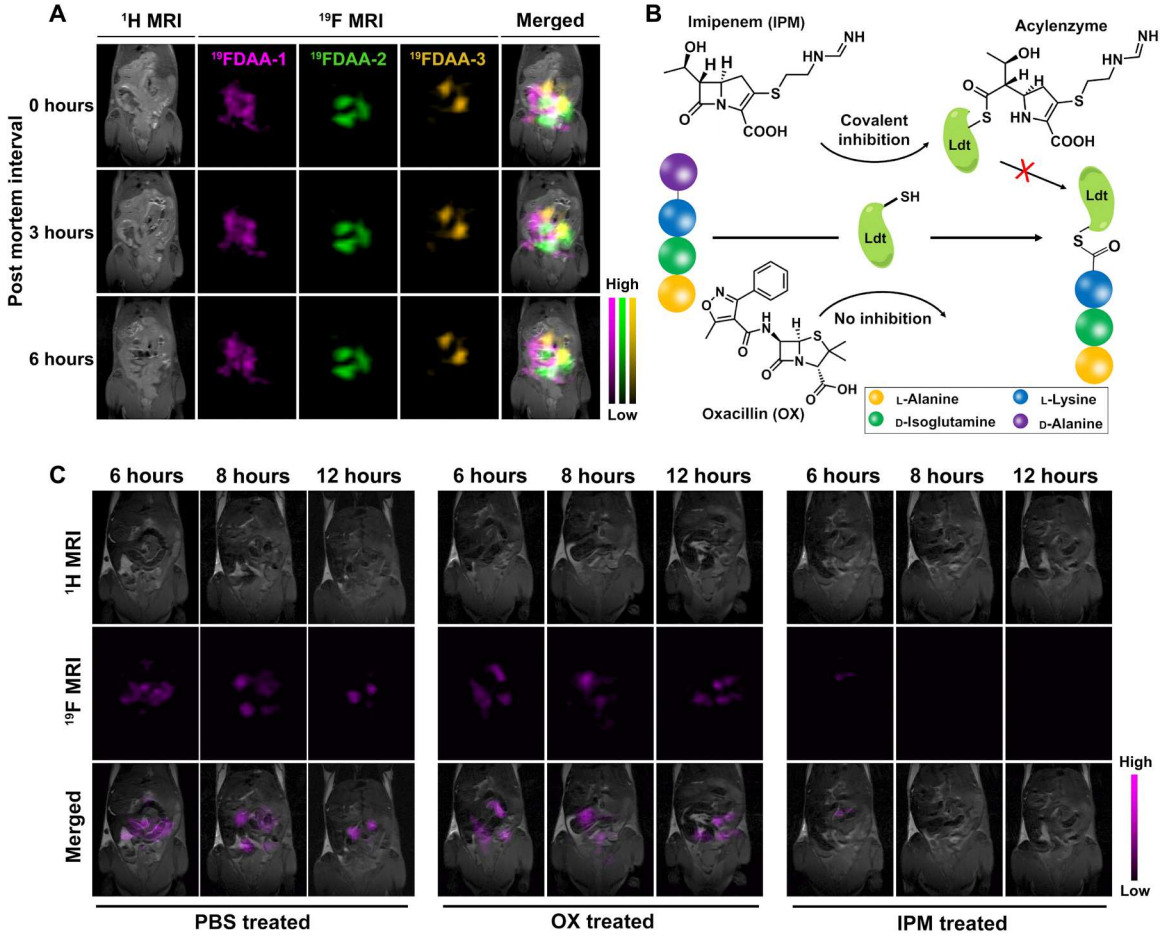

Fig. 6. Continuous monitoring of gut microbiota activities under the influences of different factors. (**A**) Continuous monitoring of the mouse gut microbiota after the host death by ^{19}F MRI. (**B**) Schematic illustration of the mechanism by which two different β-lactams influence the activity of Ldt. (**C**) ^{19}F MRI of mouse gut microbiotas treated with ^{19}F-tetraAA and an indicated β-lactam antibiotic.

introduction of the selective labeling probes toward specific groups of bacteria. Moreover, the current form of our method is not amenable to tissue-level analysis or three-dimensional imaging because of the relatively low sensitivity of ^{19}F MRI (*51*, *52*). This shortcoming could be resolved by the improvement on ^{19}F labeling efficiency (e.g., using labeling probes with more ^{19}F atoms) and signal acquisition (e.g., using body coils for more sensitive imaging), which are currently under active investigation in our laboratory.

Apart from the studies on gut microbiota, note that this approach could also be used in the studies of bacterial infections. For example, the in vivo activities of bacterial pathogens influenced by host immune system or antibacterial drugs can be continuously monitored using this method. Our strategy could be readily extended to the research of eukaryotic cells that can be metabolically labeled using appropriate ^{19}F-containing probes, such as in vivo tracking of engineered cells (e.g., chimeric antigen receptor T cells) (*53*) or even in situ labeling and in vivo monitoring of endogenous cells. We have made some promising progress along this direction. We anticipate that the further development of this approach will offer a powerful tool for multiplexed and quantitative in vivo imaging of various cells, which will pave the way for deeper understanding of the in vivo activities of prokaryotic and eukaryotic cells of interest.

MATERIALS AND METHODS

Bacterial toxicity evaluation

S. aureus American Type Culture Collection (ATCC) 29213 and *E. coli* ATCC 25922 were used as model strains for the toxicity assessment of ^{19}F-DAA and ^{19}F-LAA probes; *E. coli* ATCC 25922, *B. subtilis* China Center of Industrial Culture Collection (CICC) 23659, and *E. faecium* 28 were used for ^{19}F-tetraDAA and *ctrl*-^{19}F-tetraAA probes. The bacteria were all cultured in LB medium with shaking at 37°C overnight, except that *E. faecium* 28 was cultured in a brain heart infusion medium. Subsequently, the bacteria were incubated with ^{19}F-DAA-1, ^{19}F-DAA-2, ^{19}F-DAA-3, ^{19}F-LAA-1, ^{19}F-LAA-2, ^{19}F-LAA-3 (at a final fluorine concentration of 60 or 120 mM for DAA- and LAA-based probes), ^{19}F-tetraAA, or *ctrl*-^{19}F-tetraAA (at a final fluorine concentration of 12 or 30 mM for tetraAA-based probes) at 37°C for 3 hours. Then, the bacteria were washed with phosphate-buffered saline (PBS) thrice and resuspended in PBS. The bacterial survival was evaluated by CFU plate

counting. Corresponding bacteria without probe treatment were used as controls.

Bacterial labeling with DAA or tetrapeptide-based ^{19}F probe

To *B. subtilis* CICC 23659, *S. aureus* ATCC 29213, and *E. coli* ATCC 25922 cultured in abovementioned media, ^{19}F-DAA-1, ^{19}F-DAA-2, ^{19}F-DAA-3, and ^{19}F-tetraAA (final fluorine concentration = 1.2 mM) were added as indicated. The bacteria were incubated at 37°C for 3 hours, washed with PBS thrice, and resuspended in PBS [optical density at 600 nm (OD_{600}) = 2.5] for the following analyses.

Animal care and use statement

All animal experiments were conducted under the guidelines approved by the Institutional Animal Care and Use Committee of Xiamen University Laboratory Animal Center (reference number XMULAC20210044).

^{19}F MRI in vitro and in vivo

For in vitro, a rapid acquisition using relaxation enhancement (RARE) sequence was used to acquire ^{19}F MR images with the following parameters: center frequencies of 376.6384 MHz (−62.64 ppm), 376.6209 MHz (−109.60 ppm), and 376.6460 (−42.78 ppm); repetition time (TR) = 1200 ms; echo time (TE) = 8.5 ms; refocusing flip angle (RFA) = 180°; flip angle (FA) = 90°; field of view (FOV) = 4.0 cm by 4.0 cm; slice thickness (SI) = 10 mm; matrix = 32 × 32; and number of excitation (NEX) = 48. The total experiment time was ~5.75 min.

For in vivo, a RARE sequence was used with the following parameters: center frequencies of 376.6384 MHz (−62.64 ppm), 376.6209 MHz (−109.60 ppm), and 376.6460 (−42.78 ppm); TR = 1200 ms; TE = 8.5 ms; RFA = 180°; FA = 90°; FOV = 4.0 cm by 4.0 cm; SI = 20 mm; matrix = 32 × 32; and NEX = 96. The total acquisition time for each time point was ~11.5 min. For acquiring ^{1}H MR images, a RARE sequence was used with the following parameters: TR = 1000 ms, TE = 8.5 ms, RFA = 180°, FA = 90°, FOV = 4.0 cm by 4.0 cm, SI = 1 mm, matrix = 256 × 256, and NEX = 2. The total acquisition time for each time point was ~2.0 min.

Ex vivo ^{1}H/^{19}F MRI of gut microbiotas labeled in vivo

Six hours after gavage [^{19}F-DAA or ^{19}F-LAA probes in 200 μl of PBS at a fluorine concentration of 30 mM and ^{19}F-tetraAA or *ctrl*-^{19}F-tetraAA probe in 200 μl of PBS containing 2% dimethyl sulfoxide (DMSO) at a fluorine concentration of 42 mM], the mice were euthanized after anesthesia and their cecal microbiotas were collected. Briefly, the mouse cecum was dissected and cut into pieces with scissors in 2 ml of PBS buffer and then filtered through 40 μm cell strainers to remove nonbacterial tissues and food debris. The filtrate was centrifuged (15,000*g*, 5 min) to give bacterial pellets, which were then washed with 3× 1.5 ml of PBS, and resuspended in PBS for subsequent ^{19}F MRI analysis. No substantial impact on the metabolic activities of gut microbes was found with ^{19}F probes at the indicated concentrations (fig. S12).

Fecal microbiota transplantation

The ^{19}F-labeled cecal microbiota of donor mice collected as abovementioned was gavaged (OD_{600} = 3.6, 200 μl) to recipient mice, which were subjected to ^{19}F MRI at indicated time points.

In vivo labeling and imaging of gut microbiota with ^{19}F probes

^{19}F-DAA-1, ^{19}F-DAA-2, ^{19}F-DAA-3, ^{19}F-tetraAA, ^{19}F-DAA-1-Ac, and corresponding control probes were given to specific pathogen–free BALB/c mice via gavage (^{19}F-DAA or ^{19}F-LAA probes in 200 μl of PBS at a fluorine concentration of 30 mM and ^{19}F-tetraAA or *ctrl*-^{19}F-tetraAA probe in 200 μl of PBS containing 2% DMSO at a fluorine concentration of 42 mM), which were subjected to ^{19}F MRI at indicated time points. For GF mice, they were randomly divided into four groups and gavaged with three ^{19}F-DAA probes (dissolved in 200 μl of PBS at a fluorine concentration of 30 mM) and ^{19}F-tetraAA (dissolved in 200 μl of PBS containing 2% DMSO at a fluorine concentration of 42 mM) in a GF environment and subjected to ^{19}F MRI 6 hours later.

^{19}F MRI monitoring gut microbiota activity under the influence of different factors

For Fig. 6A, BALB/c mice were gavaged with ^{19}F-DAA-1, ^{19}F-DAA-2, and ^{19}F-DAA-3 (dissolved in 200 μl of PBS at a fluorine concentration of 30 mM) at 6-hour intervals and euthanized 18 hours after the last gavage. The mice were kept at 37°C after death and subjected to ^{19}F MRI at indicated time points. For Fig. 6C, BALB/c mice were gavaged with OX or IPM (160 μg ml^{-1}) mixed with ^{19}F-tetraAA (dissolved in 200 μl of PBS containing 2% DMSO at a fluorine concentration of 42 mM). Mice gavaged with ^{19}F-tetraAA and PBS (dissolved in 200 μl of PBS containing 2% DMSO at a fluorine concentration of 42 mM) were used as control. The mice were then subjected to ^{19}F MRI at indicated time points.

Quantification and statistical analysis

For in vitro ^{19}F MR images, the region of interest (ROI) was the effective region of sample, and the corresponding average SNR was assessed by ImageJ software. For in vivo ^{19}F MR image, the ROI was the region of stomach or intestine unless otherwise mentioned, and the average SNR was assessed similarly by ImageJ software. Unless stated otherwise, all the results are presented as means ± SD from at least three independent replicates (in vitro experiments: $n = 5$ per group; in vivo experiments: $n = 3$ per group). For statistical comparisons, Student's t tests were used (n.s., not significant; $^{*}P < 0.05$, $^{**}P < 0.01$, and $^{***}P < 0.001$). A P value $^{*} < 0.05$ was considered statistically significant.

Supplementary Materials

This PDF file includes:

Figs. S1 to S19
Tables S1 and S2
NMR Spectra

View/request a protocol for this paper from *Bio-protocol*.

REFERENCES AND NOTES

1. B. W. Ji, R. U. Sheth, P. D. Dixit, K. Tchourine, D. Vitkup, Macroecological dynamics of gut microbiota. *Nat. Microbiol.* **5**, 768–775 (2020).

2. T. Korem, D. Zeevi, J. Suez, A. Weinberger, T. Avnit-Sagi, M. Pompan-Lotan, E. Matot, G. Jona, A. Harmelin, N. Cohen, A. Sirota-Madi, C. A. Thaiss, M. Pevsner-Fischer, R. Sorek, R. Xavier, E. Elinav, E. Segal, Growth dynamics of gut microbiota in health and disease inferred from single metagenomic samples. *Science* **349**, 1101–1106 (2015).
3. E. A. Eloe-Fadrosh, A. Brady, J. Crabtree, E. F. Drabek, B. Ma, A. Mahurkar, J. Ravel, M. Haverkamp, A.-M. Fiorino, C. Botelho, I. Andreyeva, P. L. Hibberd, C. M. Fraser, Functional dynamics of the gut microbiome in elderly people during probiotic consumption. *MBio* **6**, e00231–e00215 (2015).
4. R. K. Weersma, A. Zhernakova, J. Fu, Interaction between drugs and the gut microbiome. *Gut* **69**, 1510–1519 (2020).
5. L. A. David, C. F. Maurice, R. N. Carmody, D. B. Gootenberg, J. E. Button, B. E. Wolfe, A. V. Ling, A. S. Devlin, Y. Varma, M. A. Fischbach, S. B. Biddinger, R. J. Dutton, P. J. Turnbaugh, Diet rapidly and reproducibly alters the human gut microbiome. *Nature* **505**, 559–563 (2014).
6. W. Wang, Q. Yang, Y. Du, X. Zhou, X. Du, Q. Wu, L. Lin, Y. Song, F. Li, C. Yang, W. Tan, Metabolic labeling of peptidoglycan with NIR-II dye enables *in vivo* imaging of gut microbiota. *Angew. Chem. Int. Ed. Engl.* **59**, 2628–2633 (2020).
7. J. Schluter, J. U. Peled, B. P. Taylor, K. A. Markey, M. Smith, Y. Taur, R. Niehus, A. Staffas, A. Dai, E. Fontana, L. A. Amoretti, R. J. Wright, S. Morjaria, M. Fenelus, M. S. Pessin, N. J. Chao, M. Lew, L. Bohannon, A. Bush, A. D. Sung, T. M. Hohl, M.-A. Perales, M. R. M. van den Brink, J. B. Xavier, The gut microbiota is associated with immune cell dynamics in humans. *Nature* **588**, 303–307 (2020).
8. S. Rakoff-Nahoum, K. R. Foster, L. E. Comstock, The evolution of cooperation within the gut microbiota. *Nature* **533**, 255–259 (2016).
9. A. Ostovar, M. Assadi, K. Vahdat, I. Nabipour, H. Javadi, M. Eftekhari, M. Assadi, A pooled analysis of diagnostic value of ^{99m}Tc-ubiquicidin (UBI) scintigraphy in detection of an infectious process. *Clin. Nucl. Med.* **38**, 413–416 (2013).
10. M. van Oosten, T. Schäfer, J. A. Gazendam, K. Ohlsen, E. Tsompanidou, M. C. de Goffau, H. J. Harmsen, L. M. Crane, E. Lim, K. P. Francis, L. Cheung, M. Olive, V. Ntziachristos, J. M. van Dijl, G. M. van Dam, Real-time *in vivo* imaging of invasive- and biomaterial-associated bacterial infections using fluorescently labelled vancomycin. *Nat. Commun.* **4**, 2584 (2013).
11. M. M. Welling, A. W. Hensbergen, A. Bunschoten, A. H. Velders, M. Roestenberg, F. W. B. van Leeuwen, An update on radiotracer development for molecular imaging of bacterial infections. *Clin. Transl. Imaging* **7**, 105–124 (2019).
12. A. Kaul, P. P. Hazari, H. Rawat, B. Singh, T. C. Kalawat, S. Sharma, A. K. Babbar, A. K. Mishra, Preliminary evaluation of technetium-99m-labeled ceftriaxone: Infection imaging agent for the clinical diagnosis of orthopedic infection. *Int. J. Infect. Dis.* **17**, e263–e270 (2013).
13. Z. Zhang, D. Xu, J. Fang, D. Wang, J. Zeng, X. Liu, S. Hong, Y. Xue, X. Zhang, X. Zhao, *In situ* live imaging of gut microbiota. *mSphere* **6**, e0054521 (2021).
14. C. A. Mutch, A. A. Ordonez, H. Qin, M. Parker, L. E. Bambarger, J. E. Villanueva-Meyer, J. Blecha, V. Carroll, C. Taglang, R. Flavell, R. Sriram, H. VanBrocklin, O. Rosenberg, M. A. Ohliger, S. K. Jain, K. D. Neumann, D. M. Wilson, [^{11}C]Para-aminobenzoic acid: A positron emission tomography tracer targeting bacteria-specific metabolism. *ACS Infect. Dis.* **4**, 1067–1072 (2018).
15. Z. Zhang, A. A. Ordonez, H. Wang, Y. Li, K. R. Gogarty, E. A. Weinstein, F. Daryaee, J. Merino, G. E. Yoon, A. S. Kalinda, R. C. Mease, J. N. Iuliano, P. M. Smith-Jones, S. K. Jain, P. J. Tonge, Positron emission tomography imaging with 2-[^{18}F]F-*p*-aminobenzoic acid detects *Staphylococcus aureus* infections and monitors drug response. *ACS Infect. Dis.* **4**, 1635–1644 (2018).
16. G. Gowrishankar, M. Namavari, E. B. Jouannot, A. Hoehne, R. Reeves, J. Hardy, S. S. Gambhir, Investigation of 6-[^{18}F]-fluoromaltose as a novel PET tracer for imaging bacterial infection. *PLOS ONE* **9**, e107951 (2014).
17. X. Ning, W. Seo, S. Lee, K. Takemiya, M. Rafi, X. Feng, D. Weiss, X. Wang, L. Williams, V. M. Camp, M. Eugene, W. R. Taylor, M. Goodman, N. Murthy, PET imaging of bacterial infections with fluorine-18-labeled maltohexaose. *Angew. Chem. Int. Ed. Engl.* **53**, 14096–14101 (2014).
18. G. Gowrishankar, J. Hardy, M. Wardak, M. Namavari, R. E. Reeves, E. Neofytou, A. Srinivasan, J. C. Wu, C. H. Contag, S. S. Gambhir, Specific imaging of bacterial infection using 6″-18F-fluoromaltotriose: A second-generation PET tracer targeting the maltodextrin transporter in bacteria. *J. Nucl. Med.* **58**, 1679–1684 (2017).
19. E. Kuru, H. V. Hughes, P. J. Brown, E. Hall, S. Tekkam, F. Cava, M. A. de Pedro, Y. V. Brun, M. S. VanNieuwenhze, *In situ* probing of newly synthesized peptidoglycan in live bacteria with fluorescent D-amino acids. *Angew. Chem. Int. Ed. Engl.* **51**, 12519–12523 (2012).
20. E. Kuru, A. Radkov, X. Meng, A. Egan, L. Alvarez, A. Dowson, G. Booher, E. Breukink, D. I. Roper, F. Cava, W. Vollmer, Y. Brun, M. S. VanNieuwenhze, Mechanisms of incorporation for D-amino acid probes that target peptidoglycan biosynthesis. *ACS Chem. Biol.* **14**, 2745–2756 (2019).
21. T. Nakamura, H. Matsushita, F. Sugihara, Y. Yoshioka, S. Mizukami, K. Kikuchi, Activatable ^{19}F MRI nanoparticle probes for the detection of reducing environments. *Angew. Chem. Int. Ed. Engl.* **54**, 1007–1010 (2015).
22. X. Zhu, X. Tang, H. Lin, S. Shi, H. Xiong, Q. Zhou, A. Li, Q. Wang, X. Chen, J. Gao, A fluorinated ionic liquid-based activatable ^{19}F MRI platform detects biological targets. *Chem* **6**, 1134–1148 (2020).
23. I. Ashur, H. Allouche-Arnon, A. Bar-Shir, Calcium fluoride nanocrystals: Tracers for *in vivo* ^{19}F magnetic resonance imaging. *Angew. Chem. Int. Ed. Engl.* **57**, 7478–7482 (2018).
24. E. T. Ahrens, R. Flores, H. Xu, P. A. Morel, *In vivo* imaging platform for tracking immunotherapeutic cells. *Nat. Biotechnol.* **23**, 983–987 (2005).
25. S. Bo, Y. Yuan, Y. Chen, Z. Yang, S. Chen, X. Zhou, Z.-X. Jiang, *In vivo* drug tracking with ^{19}F MRI at therapeutic dose. *Chem. Commun.* **54**, 3875–3878 (2018).
26. J. Ruiz-Cabello, B. P. Barnett, P. A. Bottomley, J. W. M. Bulte, Fluorine (^{19}F) MRS and MRI in biomedicine. *NMR Biomed.* **24**, 114–129 (2011).
27. H. Lin, X. Tang, A. Li, J. Gao, Activatable ^{19}F MRI nanoprobes for visualization of biological targets in living subjects. *Adv. Mater.* **33**, e2005657 (2021).
28. D. Xie, M. Yu, R. T. Kadakia, E. L. Que, ^{19}F magnetic resonance activity-based sensing using paramagnetic metals. *Acc. Chem. Res.* **53**, 2–10 (2020).
29. I. Tirotta, V. Dichiarante, C. Pigliacelli, G. Cavallo, G. Terraneo, F. B. Bombelli, P. Metrangolo, G. Resnati, ^{19}F magnetic resonance imaging (MRI): From design of materials to clinical applications. *Chem. Rev.* **115**, 1106–1129 (2015).
30. K. C. Partlow, J. Chen, J. A. Brant, A. M. Neubauer, T. E. Meyerrose, M. H. Creer, J. A. Nolta, S. D. Caruthers, G. M. Lanza, S. A. Wickline, ^{19}F magnetic resonance imaging for stem/progenitor cell tracking with multiple unique perfluorocarbon nanobeacons. *FASEB J.* **21**, 1647–1654 (2007).
31. C. Chirizzi, D. De Battista, I. Tirotta, P. Metrangolo, G. Comi, F. B. Bombelli, L. Chaabane, Multispectral MRI with dual fluorinated probes to track mononuclear cell activity in mice. *Radiology* **291**, 351–357 (2019).
32. K. Akazawa, F. Sugihara, T. Nakamura, H. Matsushita, H. Mukai, R. Akimoto, M. Minoshima, S. Mizukami, K. Kikuchi, Perfluorocarbon-based ^{19}F MRI nanoprobes for *in vivo* multicolor imaging. *Angew. Chem. Int. Ed. Engl.* **57**, 16742–16747 (2018).
33. A. Li, X. Luo, L. Li, D. Chen, X. Liu, Z. Yang, L. Yang, J. Gao, H. Lin, Activatable multiplexed ^{19}F magnetic resonance imaging visualizes reactive oxygen and nitrogen species in drug-induced acute kidney injury. *Anal. Chem.* **93**, 16552–16561 (2021).
34. D. Cohen, R. Mashiach, L. Houben, A. Galisova, Y. Addadi, D. Kain, A. Lubart, P. Blinder, H. Allouche-Arnon, A. Bar-Shir, Glyconanofluorides as immunotracers with a tunable core composition for sensitive hotspot magnetic resonance imaging of inflammatory activity. *ACS Nano* **15**, 7563–7574 (2021).
35. X. Zhu, H. Xiong, S. Wang, Y. Li, J. Chi, X. Wang, T. Li, Q. Zhou, J. Gao, S. Shi, Fluorinated ionic liquid based multicolor ^{19}F MRI nanoprobes for *in vivo* sensing of multiple biological targets. *Adv. Healthc. Mater.* **11**, e2102079 (2021).
36. R. Chen, J. Song, L. Lin, J. Liu, C. Yang, W. Wang, Visualizing the growth and division of rat gut bacteria by D-amino acid-based *in vivo* labeling and FISH staining. *Front. Mol. Biosci.* **8**, 681938 (2021).
37. L. Lin, Q. Wu, J. Song, Y. Du, J. Gao, Y. Song, W. Wang, C. Yang, Revealing the *in vivo* growth and division patterns of mouse gut bacteria. *Sci. Adv.* **6**, eabb2531 (2020).
38. A. C. Brown, A. Valiere, Probiotics and medical nutrition therapy. *Nutr. Clin. Care* **7**, 56–68 (2004).
39. G. Reid, Safe and efficacious probiotics: What are they? *Trends Microbiol.* **14**, 348–352 (2006).
40. J. Suez, N. Zmora, E. Segal, E. Elinav, The pros, cons, and many unknowns of probiotics. *Nat. Med.* **25**, 716–729 (2019).
41. W. Wang, N. Zhang, Y. Du, J. Gao, M. Li, L. Lin, D. M. Czajkowsky, X. Li, C. Yang, Z. Shao, Three-dimensional quantitative imaging of native microbiota distribution in the gut. *Angew. Chem. Int. Ed. Engl.* **60**, 3055–3061 (2021).
42. S. E. Pidgeon, A. J. Apostolos, J. M. Nelson, M. Shaku, B. Rimal, M. N. Islam, D. C. Crick, S. J. Kim, M. S. Pavelka, B. D. Kana, M. M. Pires, L,D-Transpeptidase specific probe reveals spatial activity of peptidoglycan cross-linking. *ACS Chem. Biol.* **14**, 2185–2196 (2019).
43. H. Lin, L. Lin, Y. Du, J. Gao, C. Yang, W. Wang, Biodistributions of L,D-transpeptidases in gut microbiota revealed by *in vivo* labeling with peptidoglycan analogs. *ACS Chem. Biol.* **16**, 1164–1171 (2021).
44. L. Lin, J. Song, Y. Du, Q. Wu, J. Gao, Y. Song, C. Yang, W. Wang, Quantification of bacterial metabolic activities in the gut by D-amino acid-based *in vivo* labeling. *Angew. Chem. Int.* **59**, 11923–11926 (2020).
45. J. L. Metcalf, Z. Z. Xu, S. Weiss, S. Lax, W. Van Treuren, E. R. Hyde, S. J. Song, A. Amir, P. Larsen, N. Sangwan, D. Haarmann, G. C. Humphrey, G. Ackermann, L. R. Thompson, C. Lauber, A. Bibat, C. Nicholas, M. J. Gebert, J. F. Petrosino, S. C. Reed, J. A. Gilbert, A. M. Lynne, S. R. Bucheli, D. O. Carter, R. Knight, Microbial community assembly and metabolic function during mammalian corpse decomposition. *Science* **351**, 158–162 (2016).
46. H. Lutz, A. Vangelatos, N. Gottel, A. Osculati, S. Visona, S. J. Finley, J. A. Gilbert, G. T. Javan, Effects of extended postmortem interval on microbial communities in organs of the human cadaver. *Front. Microbiol.* **11**, 569630 (2020).

47. S. Becattini, Y. Taur, E. G. Pamer, Antibiotic-induced changes in the intestinal microbiota and disease. *Trends Mol. Med.* **22**, 458–478 (2016).
48. G. Ianiro, H. Tilg, A. Gasbarrini, Antibiotics as deep modulators of gut microbiota: Between good and evil. *Gut* **65**, 1906–1915 (2016).
49. P. V. Khodakivskyi, C. L. Lauber, A. Yevtodiyenko, A. A. Bazhin, S. Bruce, T. Ringel-Kulka, Y. Ringel, B. Bétrisey, J. Torres, J. Hu, C. J. Chou, E. A. Goun, Noninvasive imaging and quantification of bile salt hydrolase activity: From bacteria to humans. *Sci. Adv.* **7**, eaaz9857 (2021).
50. P. Kumar, A. Kaushik, E. P. Lloyd, S. G. Li, R. Mattoo, N. C. Ammerman, D. T. Bell, A. L. Perryman, T. A. Zandi, S. Ekins, S. L. Ginell, C. A. Townsend, J. S. Freundlich, G. Lamichhane, Non-classical transpeptidases yield insight into new antibacterials. *Nat. Chem. Biol.* **13**, 54–61 (2017).
51. M. J. Couch, I. K. Ball, T. Li, M. S. Fox, S. L. Littlefield, B. Biman, M. S. Albert, Pulmonary ultrashort echo time ^{19}F MR imaging with inhaled fluorinated gas mixtures in healthy volunteers: Feasibility. *Radiology* **269**, 903–909 (2013).
52. C. Constantinides, M. L. Maguire, L. Stork, E. Swider, M. Srinivas, C. A. Carr, J. E. Schneider, Temporal accumulation and localization of isoflurane in the C57BL/6 mouse and assessment of its potential contamination in ^{19}F MRI with perfluoro-crown-ether-labeled cardiac progenitor cells at 9.4 Tesla. *J. Magn. Reson. Imaging* **45**, 1659–1667 (2017).
53. H. J. Jackson, S. Rafiq, R. J. Brentjens, Driving CAR T-cells forward. *Nat. Rev. Clin. Oncol.* **13**, 370–383 (2016).

Acknowledgments: We thank Prof. X. Zhou and Prof. S. Chen at the Innovation Academy for Precision Measurement Science and Technology, Chinese Academy of Sciences for the help on the imaging of GF mice. **Funding:** We acknowledge the research support from the National Natural Science Foundation of China (22125702, 22122702, 22077107, and 92059109), the Natural Science Foundation of Fujian Province of China (2020J02001), the Youth Innovation Funding Program of Xiamen City (3502Z20206051), and the Innovative Research Team of High-Level Local Universities in Shanghai (SSMU-ZLCX20180701). **Author contributions:** J.Ga., D.C., Hongyu Lin, C.Y., and W.W. designed the study. D.C. and J.Gu. performed the experiments and analyzed the data. A.L. and C.S. took part in the design of partial experiments. Hongyu Lin, D.C., J.Gu., W.W., and J.Ga. prepared the manuscript. Huibin Lin contributed intellectually to the analysis and interpretation of the data. Hongyu Lin, C.Y., W.W., and J.Ga. supervised the project. All the authors have discussed and approved the final version of the manuscript. **Competing interests:** The authors declare that they have no competing interests. **Data and materials availability:** All data needed to evaluate the conclusions in the paper are present in the paper and/or the Supplementary Materials.

Submitted 8 April 2022
Accepted 23 December 2022
Published 27 January 2023
10.1126/sciadv.abg6808